JCTC Journal of Chemical Theory and Computation

pubs.acs.org/JCTC Article

Physics-Constrained Hardware-Efficient Ansatz on Quantum Computers That Is Universal, Systematically Improvable, and Size-Consistent

Xiaoxiao Xiao, Hewang Zhao, Jiajun Ren, Wei-Hai Fang, and Zhendong Li*

Cite This: J. Chem. Theory Comput. 2024, 20, 1912−1922 Read Online

ACCESS | Metrics & More | Article Recommendations | Supporting Information

ABSTRACT: Variational wave function ansätze are at the heart of solving quantum many-body problems in physics and chemistry. Previous designs of hardware-efficient ansatz (HEA) on quantum computers are largely based on heuristics and lack rigorous theoretical foundations. In this work, we introduce a physics-constrained approach for designing HEA with rigorous theoretical guarantees by imposing a few fundamental constraints. Specifically, we require that the target HEA to be universal, systematically improvable, and size-consistent, which is an important concept in quantum many-body theories for scalability but has been overlooked in previous designs of HEA. We extend the notion of size-consistency to HEA and present a concrete realization of HEA that satisfies all these fundamental constraints while only requiring linear qubit connectivity. The developed physics-constrained HEA is superior to other heuristically designed HEA in terms of both accuracy and scalability, as demonstrated numerically for the Heisenberg model and some typical molecules. In particular, we find that restoring size-consistency can significantly reduce the number of layers needed to reach a certain accuracy. In contrast, the failure of other HEA to satisfy these constraints severely limits their scalability to larger systems with more than 10 qubits. Our work highlights the importance of incorporating physical constraints into the design of HEA for efficiently solving many-body problems on quantum computers.

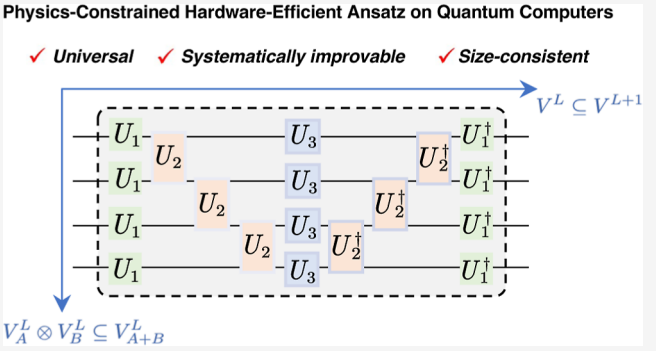

INTRODUCTION

Efficient simulation of quantum many-body problems is an enduring frontier in computational physics and chemistry.[1] Among many different approaches, the variational method represents a powerful and versatile technique to tackle quantum many-body problems. A wealth of variational wave function ansätze on classical computers have been developed over the past decades. Prominent examples include Slater determinants, Gutzwiller wave function,[2] Jastrow wave function,[3] tensor network states,[4−10] and neural network (NN) states.[11−17] Thanks to the rapid progress on quantum hardware,[18,19] the variational quantum eigensolver (VQE),[20,21] which is a hybrid quantum-classical approach for solving quantum many-body problems,[22] has attracted much attention.[23−26] The central component of VQE is the preparation of a trial wave function on quantum computers, which ultimately determines the accuracy of the variational computation. Compared to the development of variational ansätze on classical computers, the exploration of wave function ansätze on quantum computers is still in its infancy.

Available variational ansätze on quantum computers developed so far can be broadly classified into two categories: physics/chemistry-inspired ansätze and hardware-efficient ansätze (HEA), each with its own advantages and disadvantages. The chemistry-inspired unitary coupled cluster (UCC) ansatz[27] is the first ansatz proposed for determining molecular ground states on quantum computers,[20] which is motivated by the great success of the traditional coupled cluster theory on classical computers.[28] However, it quickly becomes impractical for large molecules on the current noisy intermediate-scale quantum hardware[29] since the circuit depth scales as $O(N^4)$ with respect to the number of qubits N.[30−32] Many efforts have been devoted to reduce the complexity of UCC, resulting in several descendants of UCC such as the unitary paired CC ansatz,[33] the unitary cluster Jastrow ansatz,[34] and some adaptive variants.[35−38] Another type of physics-inspired ansatz is the Hamiltonian variational ansätz (HVA),[39,40] which is problem specific and widely used for model systems.[41] When applied to

Received: September 1, 2023
Revised: January 23, 2024
Accepted: January 24, 2024
Published: February 14, 2024

https://doi.org/10.1021/acs.jctc.3c00966
J. Chem. Theory Comput. 2024, 20, 1912−1922

general cases, such as the molecular Hamiltonian in quantum chemistry, it suffers from the same problem as UCC.

HEA were originally proposed as a more practical alternative on near-term quantum devices.[42] It takes the following form

$$|\Psi\rangle = U_L(\vec{\theta}_L)\ldots U_1(\vec{\theta}_1)|\Phi_0\rangle \triangleq \prod_{l=1}^{L} U_l(\vec{\theta}_l)|\Phi_0\rangle \tag{1}$$

where $|\Phi_0\rangle$ is a reference state and the repeating unit $U_l(\vec{\theta}_l)$ is a parametrized quantum circuit composed of gates that are native on quantum hardware,[42] such as single-qubit rotation gates and two-qubit entangling gates (see Figure 1a). Given the hardware

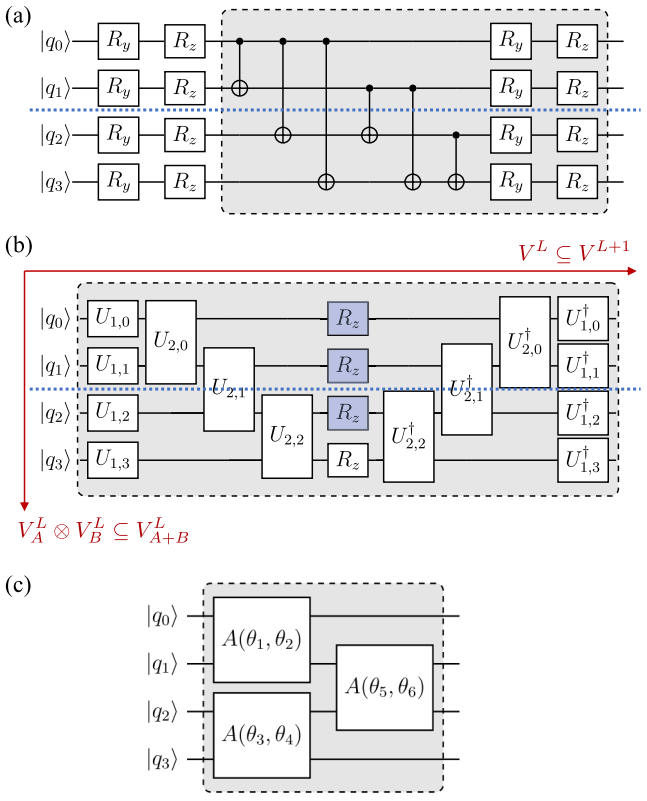

Figure 1. Heuristically designed HEA and physics-constrained HEA. (a) R_yR_z full (EfficientSU2) ansatz. The R_y full ansatz can be obtained by removing the columns of R_z gates, while the R_y linear ansatz can be derived from the R_y full ansatz by further replacing the all-to-all CNOT gates by nearest neighbor CNOT gates. (b) XYZ1F (gates in white) and XYZ2F (gates in white and blue) ansätze. The dashed box indicates a single repeating unit $U_l(\vec{\theta}_l)$, and all the parameters are omitted for brevity. The two inclusion constraints $V^L \subseteq V^{L+1}$ and $V_A^L \otimes V_B^L \subseteq V_{A+B}^L$ for extending HEA in different directions of quantum circuits are highlighted. The blue dashed line represents a partition of the whole system into two subsystems A and B. (c) Example of particle-number conserving ansatz introduced in refs 57 and 58.

constraints, there is still a great deal of freedom in choosing the layout of the circuit block $U_l(\vec{\theta}_l)$. So far, the architectures of HEA have been designed mostly by heuristics, and there is no theoretical guarantee for their performance. Furthermore, the optimization of HEA is challenging[43] as the number of qubits N and the number of layers L increase due to the proliferation of low-quality local minima[44] and the exponential vanishing of gradients, known as the "barren plateau" phenomenon.[45] These problems severely limit the scalability of HEA beyond small systems. Therefore, it is highly desirable to design a variational ansatz with rigorous theoretical basis, while at the same time being hardware-efficient on near-term devices.[46,47]

In this work, we present a new way to design HEA with rigorous theoretical guarantees by imposing fundamental constraints. This is inspired by the remarkably successful way to design exchange−correlation (XC) functionals in density functional theory (DFT) by requiring the XC functionals to satisfy exact constraints,[48] which has led to reliable nonempirical XC functionals for a wide range of systems.[49,50] We expect that designing HEA in a similar way can lead to more systematic construction of variational ansätze on quantum computers. The remaining part of the article is organized as follows: first, we introduce some fundamental constraints for HEA. Specifically, we require the ansatz to be universal, systematically improvable, and size-consistent (or multiplicatively separable), which is an important property for scalability in quantum many-body theory. Then, we present one concrete realization that satisfies all these requirements while requiring only linear qubit connectivity with nearest neighbor interactions. Consequently, a layerwise optimization strategy is introduced to take full advantage of the systematic improvability of the proposed ansatz, which is shown to alleviate the barren plateau problem. The effectiveness of this ansatz is demonstrated for the Heisenberg model and some typical molecules. The comparison with other HEA shows that incorporating physical constraints into the design of HEA is a promising way to design more efficient and scalable variational ansätze on quantum computers.

THEORY AND ALGORITHM

Fundamental Constraints for HEA. We first introduce some fundamental constraints that a good HEA should satisfy. Given a system A, suppose the variational space of HEA with L layers in eq 1 is denoted by V_A^L, we impose the following four basic constraints for the possible form of $U_l(\vec{\theta}_l)$:

(1) Universality: any quantum state should be approximated arbitrarily well by the designed HEA with a sufficiently large number of layers L.

(2) Systematic improvability: V_A^L should be included in V_A^{L+1} for any L, i.e., $V_A^L \subseteq V_A^{L+1}$. This guarantees that the variational space is systematically expanded, and the variational energy converges monotonically as L increases, i.e., $E_A^{L+1} \leq E_A^L$. A simple sufficient condition for the systematic improvability is that there exists a set of parameters $\vec{\theta}_l$ such that $U_l(\vec{\theta}_l) = I$.

(3) Size-consistency: since the exact wave function of a compound system $A + B$ consisting of two noninteracting subsystems A and B is multiplicatively separable, i.e., $|\Psi^{A+B}\rangle = |\Psi^A\rangle|\Psi^B\rangle$, we require that $V_A^L \otimes V_B^L$ should be included in V_{A+B}^L for any L, i.e., $V_A^L \otimes V_B^L \subseteq V_{A+B}^L$ (see Figure 1b). As the Hamiltonian of the composite system is $\hat{H}_{A+B} = \hat{H}_A + \hat{H}_B$, the constraint ensures that the variational energy E_{A+B}^L of the composite system will not be worse than the sum of the individually computed energies $E_A^L + E_B^L$, i.e., $E_{A+B}^L \leq E_A^L + E_B^L$. This size-consistency condition requires that for any $U_A(\vec{\theta}_{l,A})$ and $U_B(\vec{\theta}_{l,B})$, there exists a set of parameters $\vec{\theta}_{l,A+B}$ such that $U_{A+B}(\vec{\theta}_{l,A+B}) = U_A(\vec{\theta}_{l,A}) \otimes U_B(\vec{\theta}_{l,B})$.

(4) Noninteracting limit: in the limit that all the qubits are noninteracting, the eigenstates are given by product

https://doi.org/10.1021/acs.jctc.3c00966
J. Chem. Theory Comput. 2024, 20, 1912−1922

states. Thus, we require that for a good HEA, $L = 1$ should be sufficient for representing any product state, and hence $L > 1$ is only required for entangled states.

If we make an analogy between HEA for quantum wave function and NN for high-dimensional functions in classical computing, then the requirement (1) plays a similar role as the universal approximation theorem[51,52] for NN. As shown in Figure 1b, the two inclusion constraints (2) and (3) represent the constraints for extending HEA in two different directions of quantum circuits. To some extent, the systematic improvability is analogous to the ResNet[53] in classical NN architecture, which uses NN to parametrize the residual and enables the use of very deep NN in practice. In a similar spirit, we hope that an HEA with systematic improvability can allow the use of very deep quantum circuits. This turns out to be true as demonstrated numerically in a later section. The size-consistency constraint (3) introduced for HEA extends the notion of size-consistency/size-extensivity in quantum chemistry[54−56] for the qualification and differentiation of many-body methods. A size-extensive method such as the coupled cluster theory[55] can provide energies that grow linearly with the number of electrons in the system. This is mandatory for the application of a many-body method to large systems such as solids because it guarantees that the quality of the energy will not deteriorate compared to that for small systems. This concept is therefore also essential for the scalability of the variational ansatz on quantum computers.

Some previously designed HEA are shown in Figure 1a. The commonly used R_y and R_yR_z (EfficientSU2) ansätze with different entangling blocks[42] clearly fail to meet these important requirements, in particular, constraints (2) and (3). It is obvious that the R_y ansatz can only represent real wave functions, whereas it is unclear whether the R_yR_z ansatz is universal. Recently, a "cascade" ansatz is developed to satisfy the condition $U_l(\vec{\theta}_l) = I$ by adding the inverse of the CNOT gates in R_y ansatz into the repeating unit.[46] However, it fails to meet the constraints (3) and (4). The HVA for model systems of the form $U_l(\vec{\theta}_l) = \prod_k e^{i\theta_{l,k}\hat{H}_k}$, where $\hat{H}_k$ is a component of the Hamiltonian of the system $\hat{H} = \sum_k \hat{H}_k$, satisfies constraints (2) and (3) but does not necessarily meet constraints (1) and (4), which are requirements for general-purpose HEA. Similarly, the separable-pair approximation (SPA) ansatz[59,60] satisfies the size-consistency and is hardware-efficient but not universal. Particle-number symmetry-preserving ansätze have also been introduced. A typical example is the ASWAP ansatz,[57,58] as shown in Figure 1c, where the following exchange-type two-qubit gate $A(\theta, \phi)$ is used

$$A(\theta, \phi) = \begin{bmatrix} 1 & 0 & 0 & 0 \\ 0 & \cos\theta & e^{i\phi}\sin\theta & 0 \\ 0 & e^{-i\phi}\sin\theta & -\cos\theta & 0 \\ 0 & 0 & 0 & 1 \end{bmatrix} \tag{2}$$

Since only $|01\rangle$ and $|10\rangle$ are allowed to mix, this gate preserves the particle number of the input state with well-defined particle number. It is universal only within the Hilbert space with fixed number of electrons, but fails to satisfy the constraints (2) and (3), because the identity operator cannot be achieved by $A(\theta, \phi)$. The ansatz using the following hop gate[61]

$$h(\varphi) = \begin{bmatrix} 1 & 0 & 0 & 0 \\ 0 & \cos\varphi & -\sin\varphi & 0 \\ 0 & \sin\varphi & \cos\varphi & 0 \\ 0 & 0 & 0 & -1 \end{bmatrix} \tag{3}$$

also fails to satisfy the systematically improvability and size-consistency due to the exactly same problem. In summary, to the best of our knowledge, an HEA satisfying all of these constraints has not been proposed before. Our goal is to design an HEA satisfying these constraints and hence it will not be particle number conserving in order to be universal, which is advantageous in applications such as computing Green's functions.[62,63] For applications where the particle number is conserved, such as computing the ground state of molecules, we can apply penalties to enforce the correct particle numbers if necessary (vide post). Finally, we emphasize that apart from these theoretical constraints, since most of existing quantum devices have very restricted qubit connectivity, an additional important hardware constraint is that the building block $U_l(\vec{\theta}_l)$ should be easily implemented on quantum devices with restricted connectivity.

Physics-Constrained HEA. The above requirements still leave a lot of degree of freedom in the design of HEA. Here, we propose one possible HEA that satisfies these basic requirements, referred to as physics-constrained HEA, and only requires linear qubit connectivity. It should be pointed out that such a realization of physics-constrained HEA is not unique, and other realizations are certainly possible, which is a subject of future investigations. Our starting point is the wave function given by a product of exponential of Pauli operators

$$|\Psi\rangle = e^{i\theta_L P_L} \ldots e^{i\theta_1 P_1}|\Phi_0\rangle \triangleq \prod_{l=1}^{L} e^{i\theta_l P_l}|\Phi_0\rangle \tag{4}$$

which is the form for the UCC-type ansatz. A simple observation is that if one can choose all possible $P_l \in \{I, X, Y, Z\}^{\otimes N}$, this form of $U_l(\theta_l)$ $(=e^{i\theta_l P_l})$ is universal.[64,65] It is also systematically improvable because the choice $\theta_l = 0$ gives an identity operator. However, it does not satisfy constraints (3) and (4). Thus, if each layer of HEA has the ability to represent any $e^{i\theta_l P_l}$ with $P_l \in \{I, X, Y, Z\}^{\otimes N}$, the resulting ansatz will automatically satisfy constraints (1) and (2), and we only need to modify it to satisfy constraints (3) and (4). The fact that any $e^{i\theta_l P_l}$ can be represented by a quantum circuit with CNOT "staircases"[64] (see Figure 2a,b) motivates us to design $U_l(\vec{\theta}_l)$ with a similar structure (see Figure 2c), where the forms of the single-qubit gates U_1 and two-qubit gates U_2 remain to be specified. We find the following sufficient condition for representing any $e^{i\theta_l P_l}$ by the circuit block in Figure 2c:

Theorem 1 *If U_2 include gates in* {I, CNOT, SWAP or iSWAP}, *then the circuit block in* Figure 2c *can represent any* $e^{i\theta_l P_l}$ *with* $P_l \in \{I, Z\}^{\otimes N}$. *Furthermore, if U_1 include gates in* $\{I, R_x(\pi/2), R_y(-\pi/2)$ or $H\}$, *then the circuit block can represent any* $e^{i\theta_l P_l}$ *with* $P_l \in \{I, X, Y, Z\}^{\otimes N}$.

The proof of Theorem 1 is quite straightforward. We only give two concrete examples in Figure 2, arising from the double excitation $a_0^\dagger a_2^\dagger a_4 a_5$ and the single excitation $a_1^\dagger a_4$ in UCC, respectively. It can be easily verified that $e^{i\theta Z_0 Z_1 Z_2 Z_4 Z_5}$ in Figure 2a is given by XYZ1F in Figure 2c with $U_{2,k}$ = CNOT for $k \in \{0, 1, 3, 4\}$ and $U_{2,2}$ = SWAP/iSWAP, while $e^{i\theta Z_1 Z_2 Z_3 Z_4}$ in Figure 2b is

https://doi.org/10.1021/acs.jctc.3c00966
J. Chem. Theory Comput. 2024, 20, 1912−1922

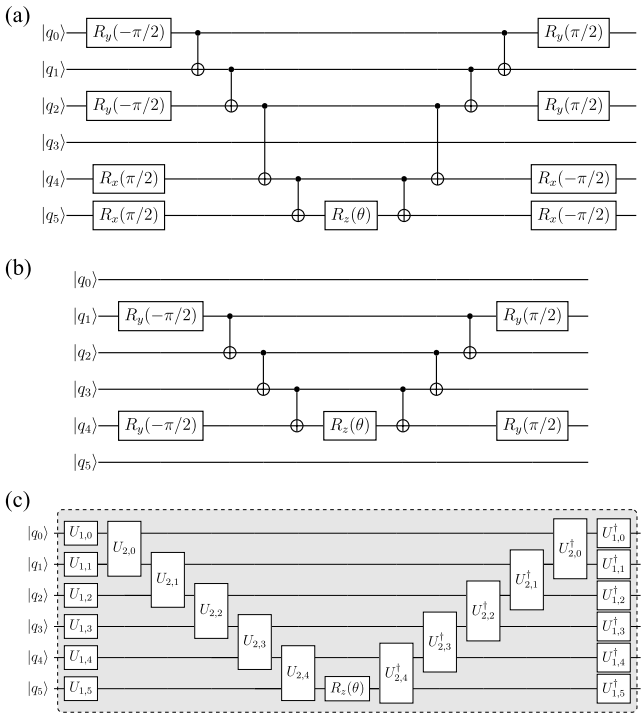

Figure 2. Examples for Theorem 1 with six qubits. (a,b) Quantum circuits appeared in UCC arising from the double excitation $a_0^\dagger a_2^\dagger a_4 a_5$ and the single excitation $a_1^\dagger a_4$, respectively; (c) XYZ1F circuit. Both (a,b) can be represented by (c) by appropriately choosing single-qubit gates $U_{1,k}$ from $\{I, R_x(\pi/2), R_y(-\pi/2)$ or $H\}$ and two-qubit gates $U_{2,k}$ from $\{I$, CNOT, SWAP or iSWAP$\}$.

given by $U_{2,0} = I$, $U_{2,k}$ = CNOT for $k \in \{1, 2, 3\}$, and $U_{2,4}$ = SWAP/iSWAP. Other $e^{i\theta P_l}$ can be represented by a similar recipe. The role of SWAP can be replaced by iSWAP, which is easier to implement on some quantum computing platforms, such as superconducting quantum devices.[66]

There are still infinitely many ways to parametrize U_1 and U_2 that satisfy this sufficient condition, since a general single-qubit (two-qubit) gate can be described by three (15) parameters, and at most three CNOT gates are needed for general two-qubit gates.[67,68] To minimize the number of parameters per circuit block and reduce the number of native two-qubit gates in U_2, here we present a parametrization of U_2 with two parameters

$$U_2(\theta, \phi) = [I \otimes R_y(\phi/2)]U_{\mathrm{fSim}}(\theta, \phi)[I \otimes R_y(-\phi/2)] \tag{5}$$

using the fSim gate $U_{\mathrm{fSim}}(\theta, \phi)$ native on some superconducting devices[69]

$$U_{\mathrm{fSim}}(\theta, \phi) = \begin{bmatrix} 1 & 0 & 0 & 0 \\ 0 & \cos\theta & -i\sin\theta & 0 \\ 0 & -i\sin\theta & \cos\theta & 0 \\ 0 & 0 & 0 & e^{-i\phi} \end{bmatrix} \tag{6}$$

which yields

$$U_2(0, 0) = I, \quad U_2(-\pi/2, 0) = \mathrm{iSWAP}, \quad U_2(0, \pi) = \mathrm{CNOT} \tag{7}$$

A simple choice for the single-qubit gates U_1 to satisfy the sufficient condition is

$$U_1(\theta, \phi) = R_x(\theta)R_y(\phi) \tag{8}$$

Equations 5 and 8 completely define a HEA, which can implement an exponential of any Pauli operator by appropriate choice of parameters. We will refer to it as XYZ1F in the following context; see Figure 2c, as an abbreviation for the combination of the three types of single-qubit rotation gates used and the two-qubit gates involving fSim gates.

It is easy to see that the XYZ1F ansatz, however, does not yet satisfy constraints (3) and (4). Fortunately, by simply replacing the single R_z gate in the middle by a layer of R_z gate, we can resolve this problem and obtain the final physics-constrained HEA, denoted by XYZ2F in Figure 1b (with additional gates in blue). The size-consistency of XYZ2F can be seen as follows: suppose the subsystems A and B contain the first two and the remaining two qubits, respectively, then the wave function $|\Psi_A^L\rangle|\Psi_B^L\rangle$ formed by a direct product of the two XYZ2F wave functions can be represented by an XYZ2F ansatz for the composite system with $U_{2,1} = I$ (see Figure 1b). Therefore, the ability of U_2 to become identity is essential from a size-consistent perspective, which is missing in other HEA shown in Figure 1a,c. It can be verified that the constraint (4) is also satisfied by simply setting all U_2 to identity, such that for the nth qubit, the circuit block gives a universal single-qubit gate[64]

$$U = R_x(\theta_0)R_y(\theta_1)R_z(\theta_2)R_y^\dagger(\theta_1)R_x^\dagger(\theta_0) \tag{9}$$

Another advantage of the size-consistent modification is that terms such as $e^{i(\theta_1 X_0 X_1 + \theta_2 X_2 Z_3 Z_4 + \theta_3 Y_5)}$ can be implemented by a single layer in XYZ2F. In contrast, $e^{i\theta_1 X_0 X_1} e^{i\theta_2 X_2 Z_3 Z_4} e^{i\theta_3 Y_5}$ needs to be implemented by three consecutive blocks in XYZ1F. This will greatly reduce the number of layers required to represent certain states, as will be shown numerically for the ground state of the Heisenberg model and some typical molecules.

In summary, the constructed XYZ2F ansatz satisfies all four fundamental constraints. The number of parameters in one layer of XYZ2F is $(5N - 2)$, where $3N$ and $2(N - 1)$ are for single-qubit and two-qubit gates, respectively. Comparing the exponential $e^{i\theta_l P_l}$ with $P_l \in \{I, X, Y, Z\}^{\otimes N}$, it is seen that all the 4^N discrete choices of P_l are now embedded into a continuous space of operators $U_l(\vec{\theta}_l)$ specified by $O(N)$ parameters. Therefore, it can be viewed as an adaptive ansatz, where the operator pool contains all 4^N Pauli operators rather than given by UCCSD as in other adaptive methods.[35−38] In Table 1, we compare different HEA in terms of the numbers of parameters N_{param}, two-qubit gates N_2, single-qubit gates N_1, and the circuit depth D as a function of layer L and number of qubits N. The number of parameters in all of them scales as $O(NL)$. One disadvantage of XYZ1F and XYZ2F is that the circuit depths of

Table 1. Comparison of Different HEA in Terms of the Numbers of Parameters N_{param}, Two-Qubit Gates N_2, Single-Qubit Gates N_1, and the Circuit Depth D as a Function of the Layer L and the Number of Qubits N[a]

ansatz	N_{param}	N_2	N_1	D $(N \geq 3, L \geq 1)$
R_y linear	$N(L + 1)$	$(N - 1)L$	$N(L + 1)$	$N + 3L - 2$
R_y full	$N(L + 1)$	$N(N - 1)L/2$	$N(L + 1)$	$NL + N + L - 2$
R_yR_z full	$2N(L + 1)$	$N(N - 1)L/2$	$2N(L + 1)$	$NL + N + 2L - 2$
ASWAP	$2(N - 1)L$	$(N - 1)L$	0	$2L$
XYZ1F	$(4N - 1)L$	$2(N - 1)L$	$(8N - 3)L$	$(4N + 3)L$
XYZ2F	$(5N - 2)L$	$2(N - 1)L$	$(9N - 4)L$	$(4N + 3)L$

[a]When counting N_2 and D, we assume that the ASWAP and fSim gates are native gates.

https://doi.org/10.1021/acs.jctc.3c00966
J. Chem. Theory Comput. 2024, 20, 1912−1922

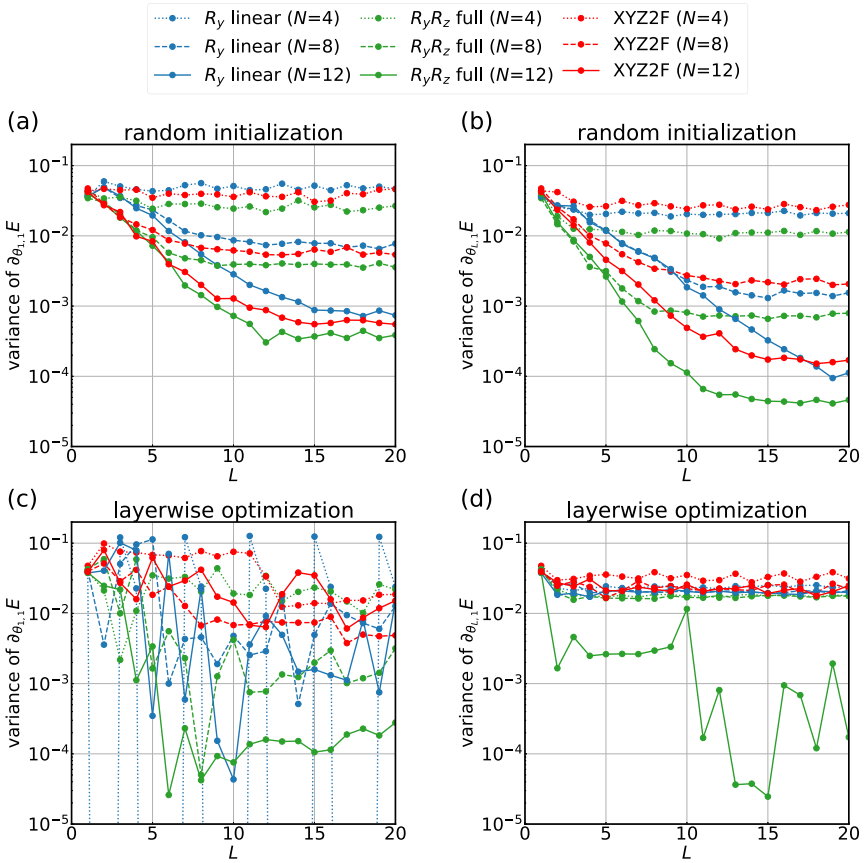

Figure 3. Variance of energy gradients for the one-dimensional Heisenberg model. (a,b) Variances of energy gradients for the first parameter in the first layer $\theta_{1,1}$ and that in the L-th layer $\theta_{L,1}$ are computed with random initialization of all parameters for 500 times. For all the HEA, an exponential vanishing of gradients with respect to the number of qubits N and the number of layers L are observed, consistent with the conclusions in ref 45. (c,d) Instead of random initialization, the parameters for the previous $L-1$ layers are the optimized parameters, while those for the L-th layer are initialized randomly for 500 times. Compared with random initialization, the layerwise optimization alleviates the barren plateau problem.

Table 2. Size-Consistency Test: Ground-State Energy per Site e_N^L and Infidelities $(1 - F_N^L$ with $F_N^L = |\langle\Psi_N^L|\Psi_N^*\rangle|^2)$ Obtained by Different HEA with $L = 2$ and $L = 4$ for a Composite Heisenberg Model (Denoted by 6 + 6), Which Consists of Two Noninteracting Subsystems with Six Sites[a]

system	R_y linear	R_y full	R_yR_z full	ASWAP	XYZ2F
$e_6^{L=2}$	−0.78333	−0.78333	−0.80606	−0.80273	−0.83054
	(0.04786)	(0.04786)	(0.02514)	(0.02846)	(**0.00065**)
$e_{6+6}^{L=2}$	−0.52002	−0.51368	−0.64791	−0.52267	−0.83054
	(0.31118)	(0.31751)	(0.18328)	(0.30853)	(**0.00065**)
$e_6^{L=4}$	−0.82988	−0.82988	−0.83089	−0.83119	−0.83119
	(0.00132)	(0.00132)	(0.00030)	(0.00000)	(**0.00000**)
$e_{6+6}^{L=4}$	−0.33247	−0.35020	−0.53154	−0.63073	−0.83119
	(0.49873)	(0.48099)	(0.29966)	(0.20047)	(**0.00000**)
$1 - F_6^{L=2}$	0.17623	0.17623	0.03743	0.05260	**0.00085**
$1 - F_{6+6}^{L=2}$	0.77773	1.00000	1.00000	0.95358	**0.00170**
$1 - F_6^{L=4}$	0.00205	0.00205	0.00037	0.00000	**0.00000**
$1 - F_{6+6}^{L=4}$	0.93368	1.00000	0.93196	0.79871	**0.00000**

[a]The parameters of the total system are taken from the optimized parameters of the subsystems. Errors with respect to the exact e_N^* obtained from exact diagonalization are shown in parentheses. Only XYZ2F satisfies $e_{6+6}^L = e_6^L$, while other HEA are not size-consistent.

XYZ1F and XYZ2F are larger than those of other HEA due to the use of the staircase structure. In principle, other low-depth architectures such as the brickwall structure can be used in the construction of physics-constrained HEA. We are exploring such possibility, and the results will be reported elsewhere.

Layerwise Optimization Algorithm. To take full advantage of the systematic improvability of XYZ1F and XYZ2F, the parameters in HEA are optimized in a layerwise way using Algorithm 1. This is different from optimization with random initialization for all parameters, which has been shown

https://doi.org/10.1021/acs.jctc.3c00966
J. Chem. Theory Comput. 2024, 20, 1912−1922

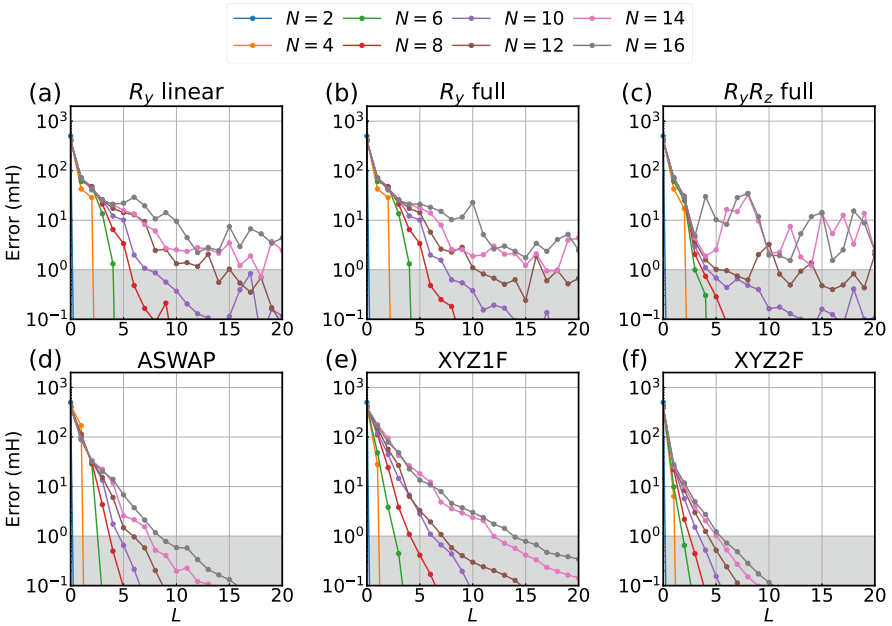

Figure 4. Convergence of the ground-state energy per site e_N^L obtained by different HEA (a: R_y linear, b: R_y full, c: R_yR_z full, d: ASWAP, e: XYZ1F, and f: XYZ2F) as a function of the number of layers L for one-dimensional antiferromagnetic Heisenberg models ($J = -1$) with different number of sites N. The exact values e_N^* are obtained from exact diagonalizations. While both XYZ1F and XYZ2F are systematically improvable, the size-consistency of XYZ2F makes it superior to XYZ1F. Other HEA do not converge monotonically and become increasingly difficult to achieve a target accuracy as the system size increases (except for ASWAP). The shaded regions represent the region within the chemical accuracy (1 mH).

to easily suffer from the problems of low-quality local minima and barren plateaus.[45] Our algorithm has two key features. First, we retain the optimized parameters from the previous step as the initial guess for the $L-1$ layers in the current step. Second, we generated n (about 10) sets of random parameters with different step sizes for the L-th layer. Each set of parameters $\vec{\theta}_L$ is obtained from $\vec{\theta}_L = \frac{\vec{u}}{\max_i |u_i|}\delta$, where $\vec{u}$ are random numbers in $[-1, 1]$ and δ is a predefined step size $\delta \in \left\{\frac{2\pi}{2^k}\right\}_{k=0}^{5} \cup \{0\}$. This guarantees that the optimized energy decreases monotonically with respect to L for XYZ1F and XYZ2F. For consistency, the layerwise optimization method is also employed in calculations using other HEA. We implement all the HEA using MindQuantum.[70] Numerical optimization in VQE employed the Broyden–Fletcher–Goldfarb–Shanno (BFGS) method implemented in Scipy.[71] As shown in the Supporting Information, during the optimization, the decrease of the energy is fast at the beginning of iterations and then slows down. Thus, we set the maximal number of iterations to be 3000 for a given layer.

Algorithm 1 Layerwise optimization strategy

Input: $L_{\max}$, $|\Phi_0\rangle$;
Initialization: $L = 0, |\Psi\rangle = |\Phi_0\rangle$;
while $L \le L_{\max}$ **do**
Set L += 1;
Generate n sets of random parameters $\{\vec{\theta}_L^{(i)}\}_{i=1}^n$ with different step sizes for the L-th layer;
Combine $\{\vec{\theta}_1, \ldots, \vec{\theta}_{L-1}\}$ obtained in the previous step as initial guess for the $L-1$ layers;
Perform n independent VQE with $|\Psi\rangle = U_L \cdots U_1|\Phi_0\rangle$ in parallel;
Collect $E_L = \min_i E_L^{(i)}$ and optimized $\{\vec{\theta}_1, \ldots, \vec{\theta}_L\}$;
end while
Output: $\{E_1, \cdots, E_{L_{\max}}\}$ and $|\Psi\rangle = U_{L_{\max}} \cdots U_1|\Phi_0\rangle$.

Figure 3 displays the variance of energy gradients for the 1D Heisenberg model (see the next section). We observe the exponential vanishing of gradients with respect to the number of qubits N and the number of layers L with random initialization, consistent with the conclusions in ref 45. In contrast, the layerwise optimization alleviates the barren plateau problem, in particular for XYZ2F.

RESULTS

Heisenberg Model. We first use the one-dimensional Heisenberg model with open boundary condition, whose Hamiltonian is $\hat{H} = -\frac{1}{2}J\sum_{n=1}^{N-1}\vec{\sigma}_n\cdot\vec{\sigma}_{n+1}$, to study the effectiveness of the constructed HEA. In Table 2, we perform a size-consistent test[54,56] for different HEA by applying them to a composite Heisenberg model (denoted by 6 + 6) consisting of two noninteracting subsystems with six sites. The parameters in the wave function of the composite system are taken from the optimized parameters for the subsystem. If an ansatz is size-consistent, then the ground-state energy per site e_N^L should be the same for the whole system and the subsystem, i.e. $e_{6+6}^L = e_6^L$ for any L. Notably, only XYZ2F satisfies this condition, while other HEA violates it significantly. The additional entangling gates between subsystems in other HEA severely degrade the quality of the approximation in the total system, as can be seen from the significant increase of infidelity $(1 - F_N^L$ with $F_N^L = |\langle\Psi_N^L|\Psi_N^*\rangle|^2$, where $|\Psi_N^*\rangle$ is the exact wave function) in Table 2. In particular, the additional CNOT gates in the R_y full ansatz (see Figure 1a) make the fidelity between the approximate state and the ground state almost vanish. On the contrary, the infidelity for XYZ2F is well-controlled, that is, if the fidelity F_6^L is $1 - \epsilon$, where ϵ is a small number (0.00085 for $L = 2$ in Table 2), then the fidelity for the total system is $(1 - \epsilon)^2$, and thus the infidelity $1 - F_{6+6}^L$ is about 2ϵ. Therefore, an interesting topic for future studies is to use parameters optimized from small systems as an initial guess of the XYZ2F for large systems.

Figure 4 shows the convergence of the ground-state energy per site e_N^L obtained by different HEA for antiferromagnetic Heisenberg models as a function of the number of layers L starting from a Néel state as reference $|\Phi_0\rangle$. We find that both

https://doi.org/10.1021/acs.jctc.3c00966
J. Chem. Theory Comput. 2024, 20, 1912−1922

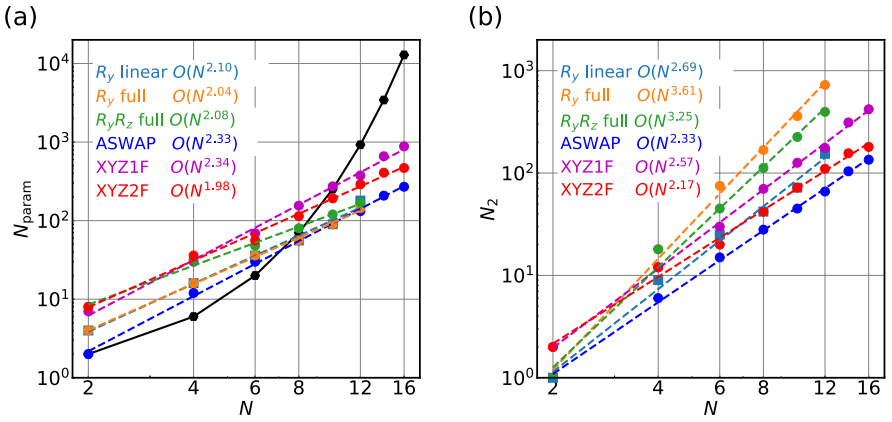

Figure 5. Number of variational parameters N_{param} (a) and the number of two-qubit gates N_2 (b) required to reach 1 milli-Hartree as a function of the number of sites N for one-dimensional antiferromagnetic Heisenberg models ($J = -1$). The dimension of the Hilbert space $\binom{N}{N/2}$ for different N is shown for comparison. The fitted scaling $O(N^b)$ is shown by dashed lines.

Table 3. Size-Consistency Test for a Composite System Composed of Two H_4 Chains (R_{H-H} = 1.5 Å) Separated by a Distance of 100 Å[a]

system	CCSD (CMO)	UCCSD (CMO)	R_y linear (OAO)	R_y full (OAO)	R_yR_z full (OAO)	ASWAP (OAO)	XYZ2F (OAO)
E_{H_4}	−1.99762 (−0.00147)	−1.99460 (0.00155)	−1.97672 (0.01943)	−1.99045 (0.00570)	−0.92429 (1.07186)	−1.99113 (0.00502)	−1.99560 **(0.00055)**
$E_{H_4-H_4}$	−3.99525 (−0.00295)	−3.98918 (0.00312)	−2.52810 (1.46420)	−2.36808 (1.62422)	−1.85371 (2.13859)	−3.48508 (0.50722)	−3.99119 **(0.00111)**
$E_{H_4-H_4} - 2E_{H_4}$	0	2.3×10^{-5}	1.43	1.61	-5.1×10^{-3}	5.0×10^{-1}	0

[a]The ground-state energies for the monomer and the entire system are obtained by classical coupled cluster singles and doubles (CCSD) and single-step Trotterized unitary CCSD (UCCSD) using canonical molecular orbitals (CMO). For HEA, the results are obtained with $L = 6$ using orthonormalized atomic orbitals (OAO). The optimized parameters for H_4 are taken as the parameters for the H_4−H_4 ladder. Errors with respect to the FCI are shown in parentheses.

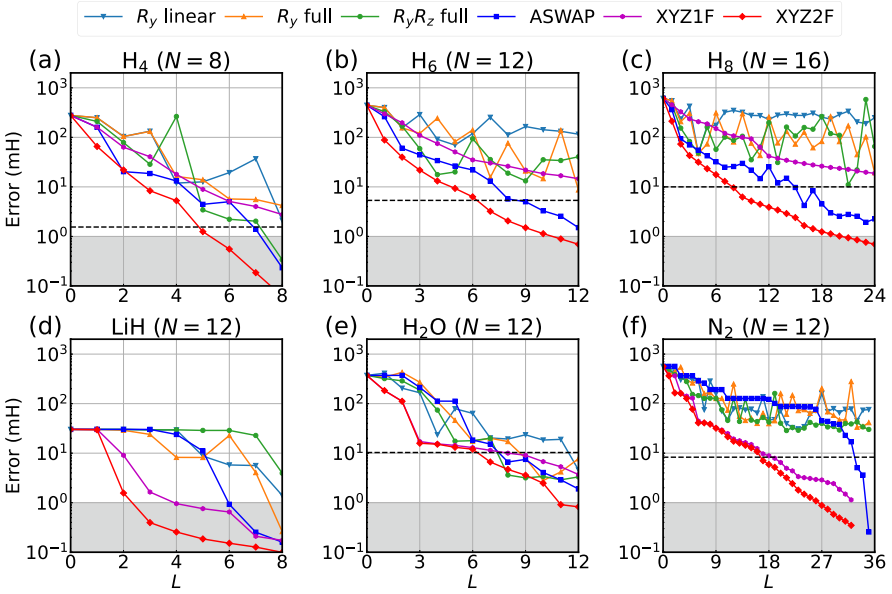

Figure 6. Ground-state energy convergence with respect to exact diagonalization results as a function of the number of layers L for molecules: (a−c) hydrogen chains (H_4, H_6, and H_8) with interatomic distance R_{H-H} = 1.5 Å; (d) LiH (R_{Li-H} = 2.0 Å); (e) H_2O (R_{O-H} = 2.0 Å and θ_{H-O-H} = 104.5°); and (f) N_2 (R_{N-N} = 2.0 Å). For H_2O, the O 1s orbital is frozen, while the N 1s and N 2s orbitals are frozen for N_2. The black dashed lines represent UCCSD results, while the shaded regions represent the region within the chemical accuracy (1 mH).

XYZ1F and XYZ2F are systematically improvable as expected, and the effect of the size-consistent modification in XYZ2F is dramatic, which significantly reduces the number of layers needed to reach a certain accuracy. In contrast, other HEA do not converge monotonically and become increasingly difficult to converge as the system size N increases (except for ASWAP). As shown in Figure 4, the oscillatory behavior reveals a severe problem of these HEA in practical applications; that is, even if

https://doi.org/10.1021/acs.jctc.3c00966
J. Chem. Theory Comput. 2024, 20, 1912−1922

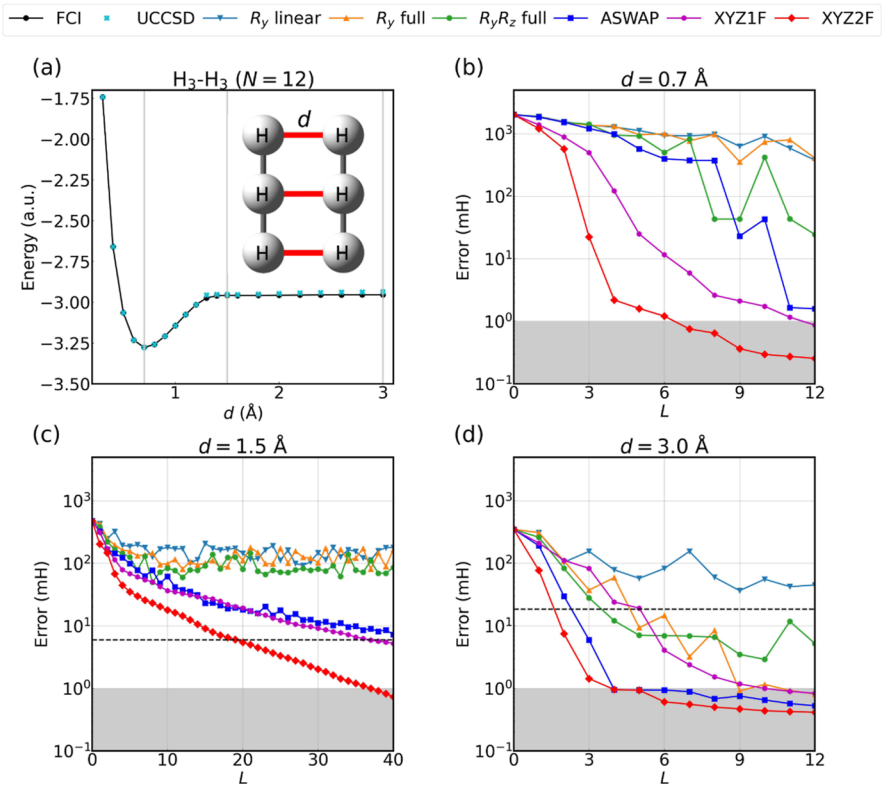

Figure 7. Two-dimensional ladder H_3−H_3 where R_{H-H} = 1.5 Å within each monomer. (a) Potential energy curve described by full configuration interaction (FCI) and unitary CCSD (UCCSD). Note that the performance of UCCSD deteriorates as d exceeds 1.3 Å. (b−d) Convergence of different HEA for the ground-state energy at three representative distances (0.7, 1.5, and 3.0 Å). The black dashed lines represent UCCSD results. The error of UCCSD at d = 0.7 Å is below 1 micro-Hartree.

they have reached a certain accuracy with L layers, the accuracy with L + 1 layers may be worse. The comparison with XYZ1F/XYZ2F suggests that it is the violation of constraints (2) and (3) that causes these heuristically designed HEA to perform poorly as N increases.

In Figure 5a, we display the number of variational parameters N_{param} to reach 1 mH as a function of the number of sites N, compared against the dimension of the Hilbert space $\binom{N}{N/2}$ for different N. It is seen that for this system, the number of variational parameters to reach 1 milli-Hartree scales as $O(N^{1.98})$ for XYZ2F. The scaling for XYZ1F and ASWAP are quite similar, but the ASWAP has a much smaller prefactor. Figure 5b shows the scaling of the number of two-qubit gates N_2 required to reach 1 milli-Hartree for different N. It is seen that XYZ2F has the lowest scaling $O(N^{2.17})$, albeit with a larger prefactor than ASWAP. Therefore, future optimization of the layout may further lead to a more economic physics-constrained HEA.

Molecules. Next we examined the performance of the constructed HEA for realistic systems. For molecules, the molecular integrals were generated using the PySCF package[72] in a minimal STO-3G basis. The Jordan−Wigner Fermion-to-qubit transformation[73] was carried out using OpenFermion,[74] where occupation number vectors (ONVs) for Fermions $|n_0 n_{\bar{0}} n_1 n_{\bar{1}} \ldots n_k n_{\bar{k}}\rangle$ ($n \in \{0, 1\}$ and the symbol $\bar{i}$ represents i-th β spin−orbital) is mapped to ONVs for qubits $|q_0 q_1 q_2 q_3 \ldots q_{2k} q_{2k+1}\rangle$.

Table 3 shows the size-consistency test for a composite hydrogen ladder composed of two H_4 chain (R_{H-H} = 1.5 Å) separated by a distance of 100 Å. It is well-known that classical spin-restricted coupled cluster singles and doubles (CCSD) method is size-consistent/extensive in this case. However, it is seen that the commonly used Trotterized unitary CCSD (UCCSD) using canonical molecular orbitals (CMO) has a small size-consistency error. Here, we consider only a single Trotter step. The Trotterization makes UCCSD lose the property of orbital invariance. Since the CMO of the H_4 ladder, which is delocalized among all hydrogen, is different from that of the H_4 monomer, the UCCSD wave function cannot be exactly factorized into a product of two wave functions. The Trotterized UCCSD can become size-consistent only with localized molecular orbitals with a proper ordering of qubits. Similarly, we can only expect size-consistency for HEA using localized orbitals. Table 3 shows the results obtained with L = 6 using orthonormalized atomic orbitals (OAO). It is clear that only XYZ2F is size-consistent in this case.

Figure 6 shows the comparison of different HEA for the convergence of ground-state energies as a function of the number of layers L for hydrogen chains (H_4, H_6, and H_8), LiH, H_2O, and N_2, which were commonly used to benchmark the performance of quantum computing techniques.[33,42,46,75,76] For the stretched hydrogen chains, the OAO were used due to the faster convergence and the reference state was a Néel state, e.g., $|\Phi_0\rangle = |10011001\rangle$ for H_4. As the number of hydrogen increases, the number of Slater determinants with large coefficients in the expansion of the exact ground state increases significantly. As shown in Figure 6, only XYZ2F converges monotonically to chemical accuracy, while other HEA perform poorly for H_6 and H_8. The number of layers needed to achieve chemical accuracy increases roughly linearly with the system size for XYZ2F.

For LiH, H_2O, and N_2, all simulated with 12 qubits using the restricted Hartree−Fock (RHF) orbitals, the convergence

https://doi.org/10.1021/acs.jctc.3c00966
J. Chem. Theory Comput. 2024, 20, 1912−1922

behavior is quite different, reflecting the very different electronic structures. For LiH at R_{Li-H} = 2.0 Å, the exact ground state is dominated by the Hartree−Fock configuration (about 95%), and thus XYZ2F quickly reaches chemical accuracy with L = 3. For H_2O and N_2 at stretched geometries upon dissociation, which are typical examples of strong electron correlations in quantum chemistry, the convergence is slower. In the calculation of H_2O, we added a penalty term for preserving the particle number, viz. $\hat{H}' = \hat{H} + \beta(\hat{N}_\uparrow - n_\uparrow)^2 + \beta(\hat{N}_\downarrow - n_\downarrow)^2$ with β = 1.0. In the calculations of N_2, we further added a penalty for the total spin, viz. $\hat{H}' = \hat{H} + \beta(\hat{N}_\uparrow - n_\uparrow)^2 + \beta(\hat{N}_\downarrow - n_\downarrow)^2 + \beta\hat{S}_+\hat{S}_-$ with β = 1.0. For the ASWAP ansatz, a larger β = 3.0 is used; otherwise, it will not converge to the ground state. As shown in Figure 6, the number of layers required for XYZ2F to reach chemical accuracy is 11 and 27, respectively. For the most challenging molecule N_2, we find that other HEA are difficult to converge to chemical accuracy.

Finally, we test the performance of HEA on a more challenging two-dimensional system, a H_3-H_3 ladder (see Figure 7). We should mention that R_y linear, ASWAP, XYZ1F, and XYZ2F are designed to be one-dimensional, and we are working on the two-dimensional extensions. But we can examine their performance on a two-dimensional system. The convergence of different HEA for the ground-state energy at three representative distances (0.7, 1.5, and 3.0 Å) are shown in Figure 7. Both in the equilibrium (d = 0.7 Å) and in the dissociation region (d = 3.0 Å), XYZ2F converge to the chemical accuracy easily, because the systems can be viewed as close to three hydrogen molecules and two H_3, respectively. At d = 1.5 Å, which equals R_{H-H} within the monomer, the system is most difficult. We find that XYZ2F require about 37 layers to converge to the chemical accuracy, while XYZ1F and ASWAP converge much more slowly. Other HEA completely fail. It is seen that ensuring the universality, systematical improvability, and size-consistency is important for the good performance of HEA even in this challenging case. Therefore, we expect that by extending the physics-constrained HEA to two-dimensional systems, better performance can be obtained.

CONCLUSIONS

In this work, we introduced a new way to design HEA by satisfying fundamental constraints, inspired by the physics-constrained way to design nonempirical XC functionals in DFT.[48] The developed physics-constrained HEA XYZ2F is superior to other heuristically designed HEA in terms of both accuracy and scalability. In particular, numerical tests show the promise of XYZ2F for challenging realistic molecules with strong electron correlation. The better scalability of XYZ2F is attributed to the satisfaction of the systematic improvability and size-consistency. Our results suggest that incorporating physical constraints into the design of HEA is a promising path toward designing efficient variational ansätze for solving many-body problems on quantum computers.

One disadvantage of XYZ2F is its high circuit depth due to the use of the staircase structure. This stems from the requirement that the circuit block can represent any exponential of a Pauli operator, which is a sufficient condition for the universality. However, this is not a necessary condition; other conditions for the universality can be imposed, which may lead to lower circuit depth. Another very interesting direction is that while we consider only one-dimensional HEA in this work, the concepts of physics-constrained HEA can be extended to construct HEA for higher dimensions. We are exploring these directions. It is conceivable that this work will inspire other realizations of HEA that satisfy these basic constraints, probably with more interesting properties such as fewer parameters, faster convergence, better trainability, and more versatile qubit connectivity.

ASSOCIATED CONTENT

Supporting Information

The Supporting Information is available free of charge at https://pubs.acs.org/doi/10.1021/acs.jctc.3c00966.

Additional information including the energy convergence behavior of XYZ2F, convergence with respect to the number of parameters, two-qubit gates count, circuit depth, comparison of the use of different orbitals and references, and results obtained from noisy simulations (PDF)

AUTHOR INFORMATION

Corresponding Author

Zhendong Li − *Key Laboratory of Theoretical and Computational Photochemistry, Ministry of Education, College of Chemistry, Beijing Normal University, Beijing 100875, China;* orcid.org/0000-0002-0683-6293; Email: zhendongli@bnu.edu.cn

Authors

Xiaoxiao Xiao − *Key Laboratory of Theoretical and Computational Photochemistry, Ministry of Education, College of Chemistry, Beijing Normal University, Beijing 100875, China*

Hewang Zhao − *Key Laboratory of Theoretical and Computational Photochemistry, Ministry of Education, College of Chemistry, Beijing Normal University, Beijing 100875, China*

Jiajun Ren − *Key Laboratory of Theoretical and Computational Photochemistry, Ministry of Education, College of Chemistry, Beijing Normal University, Beijing 100875, China;* orcid.org/0000-0002-1508-4943

Wei-Hai Fang − *Key Laboratory of Theoretical and Computational Photochemistry, Ministry of Education, College of Chemistry, Beijing Normal University, Beijing 100875, China;* orcid.org/0000-0002-1668-465X

Complete contact information is available at: https://pubs.acs.org/10.1021/acs.jctc.3c00966

Notes

The authors declare no competing financial interest.

ACKNOWLEDGMENTS

The authors acknowledge helpful comments by Jakob Kottmann and Mario Motta. This work was supported by the National Natural Science Foundation of China (grants nos. 21973003 and 22288201) and the Fundamental Research Funds for the Central Universities.

REFERENCES

(1) Martin, R. M.; Reining, L.; Ceperley, D. M. *Interacting Electrons*; Cambridge University Press, 2016.

(2) Gutzwiller, M. C. Effect of correlation on the ferromagnetism of transition metals. *Phys. Rev. Lett.* **1963**, *10*, 159−162.

(3) Jastrow, R. Many-body problem with strong forces. *Phys. Rev.* **1955**, *98*, 1479−1484.
(4) White, S. R. Density matrix formulation for quantum renormalization groups. *Phys. Rev. Lett.* **1992**, *69*, 2863−2866.
(5) Verstraete, F.; Cirac, J. I. Renormalization algorithms for quantum-many body systems in two and higher dimensions. *arXiv* **2004**, arXiv:cond-mat/0407066. preprint
(6) Shi, Y.-Y.; Duan, L.-M.; Vidal, G. Classical simulation of quantum many-body systems with a tree tensor network. *Phys. Rev. A: At., Mol., Opt. Phys.* **2006**, *74*, 022320.
(7) Vidal, G. Class of quantum many-body states that can be efficiently simulated. *Phys. Rev. Lett.* **2008**, *101*, 110501.
(8) Verstraete, F.; Murg, V.; Cirac, J. I. Matrix product states, projected entangled pair states, and variational renormalization group methods for quantum spin systems. *Adv. Phys.* **2008**, *57*, 143−224.
(9) Schollwöck, U. The density-matrix renormalization group in the age of matrix product states. *Ann. Phys.* **2011**, *326*, 96−192.
(10) Orús, R. A practical introduction to tensor networks: Matrix product states and projected entangled pair states. *Ann. Phys.* **2014**, *349*, 117−158.
(11) Carleo, G.; Troyer, M. Solving the quantum many-body problem with artificial neural networks. *Science* **2017**, *355*, 602−606.
(12) Choo, K.; Carleo, G.; Regnault, N.; Neupert, T. Symmetries and many-body excitations with neural-network quantum states. *Phys. Rev. Lett.* **2018**, *121*, 167204.
(13) Liang, X.; Liu, W.-Y.; Lin, P.-Z.; Guo, G.-C.; Zhang, Y.-S.; He, L. Solving frustrated quantum many-particle models with convolutional neural networks. *Phys. Rev. B* **2018**, *98*, 104426.
(14) Choo, K.; Neupert, T.; Carleo, G. Two-dimensional frustrated J 1- J 2 model studied with neural network quantum states. *Phys. Rev. B* **2019**, *100*, 125124.
(15) Hibat-Allah, M.; Ganahl, M.; Hayward, L. E.; Melko, R. G.; Carrasquilla, J. Recurrent neural network wave functions. *Phys. Rev. Res.* **2020**, *2*, 023358.
(16) Sharir, O.; Levine, Y.; Wies, N.; Carleo, G.; Shashua, A. Deep autoregressive models for the efficient variational simulation of many-body quantum systems. *Phys. Rev. Lett.* **2020**, *124*, 020503.
(17) Barrett, T. D.; Malyshev, A.; Lvovsky, A. Autoregressive neural-network wavefunctions for ab initio quantum chemistry. *Nat. Mach. Intell.* **2022**, *4*, 351−358.
(18) Arute, F.; Arya, K.; Babbush, R.; Bacon, D.; Bardin, J. C.; Barends, R.; Biswas, R.; Boixo, S.; Brandao, F. G. S. L.; Buell, D. A.; Burkett, B.; Chen, Y.; Chen, Z.; Chiaro, B.; Collins, R.; Courtney, W.; Dunsworth, A.; Farhi, E.; Foxen, B.; Fowler, A.; Gidney, C.; Giustina, M.; Graff, R.; Guerin, K.; Habegger, S.; Harrigan, M. P.; Hartmann, M. J.; Ho, A.; Hoffmann, M.; Huang, T.; Humble, T. S.; Isakov, S. V.; Jeffrey, E.; Jiang, Z.; Kafri, D.; Kechedzhi, K.; Kelly, J.; Klimov, P. V.; Knysh, S.; Korotkov, A.; Kostritsa, F.; Landhuis, D.; Lindmark, M.; Lucero, E.; Lyakh, D.; Mandrà, S.; McClean, J. R.; McEwen, M.; Megrant, A.; Mi, X.; Michielsen, K.; Mohseni, M.; Mutus, J.; Naaman, O.; Neeley, M.; Neill, C.; Niu, M. Y.; Ostby, E.; Petukhov, A.; Platt, J. C.; Quintana, C.; Rieffel, E. G.; Roushan, P.; Rubin, N. C.; Sank, D.; Satzinger, K. J.; Smelyanskiy, V.; Sung, K. J.; Trevithick, M. D.; Vainsencher, A.; Villalonga, B.; White, T.; Yao, Z. J.; Yeh, P.; Zalcman, A.; Neven, H.; Martinis, J. M. Quantum supremacy using a programmable superconducting processor. *Nature* **2019**, *574*, 505−510.
(19) Wu, Y.; Bao, W.-S.; Cao, S.; Chen, F.; Chen, M.-C.; Chen, X.; Chung, T.-H.; Deng, H.; Du, Y.; Fan, D.; Gong, M.; Guo, C.; Guo, C.; Guo, S.; Han, L.; Hong, L.; Huang, H.-L.; Huo, Y.-H.; Li, L.; Li, N.; Li, S.; Li, Y.; Liang, F.; Lin, C.; Lin, J.; Qian, H.; Qiao, D.; Rong, H.; Su, H.; Sun, L.; Wang, L.; Wang, S.; Wu, D.; Xu, Y.; Yan, K.; Yang, W.; Yang, Y.; Ye, Y.; Yin, J.; Ying, C.; Yu, J.; Zha, C.; Zhang, C.; Zhang, H.; Zhang, K.; Zhang, Y.; Zhao, H.; Zhao, Y.; Zhou, L.; Zhu, Q.; Lu, C.-Y.; Peng, C.-Z.; Zhu, X.; Pan, J.-W. Strong Quantum Computational Advantage Using a Superconducting Quantum Processor. *Phys. Rev. Lett.* **2021**, *127*, 180501.
(20) Peruzzo, A.; McClean, J.; Shadbolt, P.; Yung, M.-H.; Zhou, X.-Q.; Love, P. J.; Aspuru-Guzik, A.; O'Brien, J. L. A variational eigenvalue solver on a photonic quantum processor. *Nat. Commun.* **2014**, *5*, 4213.
(21) McClean, J. R.; Romero, J.; Babbush, R.; Aspuru-Guzik, A. The theory of variational hybrid quantum-classical algorithms. *New J. Phys.* **2016**, *18*, 023023.
(22) Tilly, J.; Chen, H.; Cao, S.; Picozzi, D.; Setia, K.; Li, Y.; Grant, E.; Wossnig, L.; Rungger, I.; Booth, G. H.; et al. The variational quantum eigensolver: a review of methods and best practices. *Phys. Rep.* **2022**, *986*, 1−128.
(23) Cao, Y.; Romero, J.; Olson, J. P.; Degroote, M.; Johnson, P. D.; Kieferová, M.; Kivlichan, I. D.; Menke, T.; Peropadre, B.; Sawaya, N. P.; Sim, S.; Veis, L.; Aspuru-Guzik, A. Quantum chemistry in the age of quantum computing. *Chem. Rev.* **2019**, *119*, 10856−10915.
(24) McArdle, S.; Endo, S.; Aspuru-Guzik, A.; Benjamin, S. C.; Yuan, X. Quantum computational chemistry. *Rev. Mod. Phys.* **2020**, *92*, 015003.
(25) Bauer, B.; Bravyi, S.; Motta, M.; Chan, G. K.-L. Quantum algorithms for quantum chemistry and quantum materials science. *Chem. Rev.* **2020**, *120*, 12685−12717.
(26) Cerezo, M.; Arrasmith, A.; Babbush, R.; Benjamin, S. C.; Endo, S.; Fujii, K.; McClean, J. R.; Mitarai, K.; Yuan, X.; Cincio, L.; Coles, P. J. Variational quantum algorithms. *Nat. Rev. Phys.* **2021**, *3*, 625−644.
(27) Anand, A.; Schleich, P.; Alperin-Lea, S.; Jensen, P. W.; Sim, S.; Díaz-Tinoco, M.; Kottmann, J. S.; Degroote, M.; Izmaylov, A. F.; Aspuru-Guzik, A. A quantum computing view on unitary coupled cluster theory. *Chem. Soc. Rev.* **2022**, *51*, 1659−1684.
(28) Bartlett, R. J.; Musiał, M. Coupled-cluster theory in quantum chemistry. *Rev. Mod. Phys.* **2007**, *79*, 291−352.
(29) Preskill, J. Quantum Computing in the NISQ era and beyond. *Quantum* **2018**, *2*, 79.
(30) Whitfield, J. D.; Biamonte, J.; Aspuru-Guzik, A. Simulation of electronic structure Hamiltonians using quantum computers. *Mol. Phys.* **2011**, *109*, 735−750.
(31) Seeley, J. T.; Richard, M. J.; Love, P. J. The Bravyi-Kitaev transformation for quantum computation of electronic structure. *J. Chem. Phys.* **2012**, *137*, 224109.
(32) Hastings, M. B.; Wecker, D.; Bauer, B.; Troyer, M. Improving quantum algorithms for quantum chemistry. *Quantum Inf. Comput.* **2015**, *15*, 1−21.
(33) Lee, J.; Huggins, W. J.; Head-Gordon, M.; Whaley, K. B. Generalized unitary coupled cluster wave functions for quantum computation. *J. Chem. Theory Comput.* **2019**, *15*, 311−324.
(34) Matsuzawa, Y.; Kurashige, Y. Jastrow-type decomposition in quantum chemistry for low-depth quantum circuits. *J. Chem. Theory Comput.* **2020**, *16*, 944−952.
(35) Ryabinkin, I. G.; Yen, T.-C.; Genin, S. N.; Izmaylov, A. F. Qubit coupled cluster method: a systematic approach to quantum chemistry on a quantum computer. *J. Chem. Theory Comput.* **2018**, *14*, 6317−6326.
(36) Grimsley, H. R.; Economou, S. E.; Barnes, E.; Mayhall, N. J. An adaptive variational algorithm for exact molecular simulations on a quantum computer. *Nat. Commun.* **2019**, *10*, 3007.
(37) Tang, H. L.; Shkolnikov, V.; Barron, G. S.; Grimsley, H. R.; Mayhall, N. J.; Barnes, E.; Economou, S. E. qubit-adapt-vqe: An adaptive algorithm for constructing hardware-efficient ansätze on a quantum processor. *PRX Quantum* **2021**, *2*, 020310.
(38) Yordanov, Y. S.; Armaos, V.; Barnes, C. H.; Arvidsson-Shukur, D. R. Qubit-excitation-based adaptive variational quantum eigensolver. *Commun. Phys.* **2021**, *4*, 228.
(39) Wecker, D.; Bauer, B.; Clark, B. K.; Hastings, M. B.; Troyer, M. Gate-count estimates for performing quantum chemistry on small quantum computers. *Phys. Rev. A: At., Mol., Opt. Phys.* **2014**, *90*, 022305.
(40) Wecker, D.; Hastings, M. B.; Troyer, M. Progress towards practical quantum variational algorithms. *Phys. Rev. A: At., Mol., Opt. Phys.* **2015**, *92*, 042303.
(41) Wiersema, R.; Zhou, C.; de Sereville, Y.; Carrasquilla, J. F.; Kim, Y. B.; Yuen, H. Exploring entanglement and optimization within the hamiltonian variational ansatz. *PRX Quantum* **2020**, *1*, 020319.
(42) Kandala, A.; Mezzacapo, A.; Temme, K.; Takita, M.; Brink, M.; Chow, J. M.; Gambetta, J. M. Hardware-efficient variational quantum

eigensolver for small molecules and quantum magnets. *Nature* **2017**, *549*, 242−246.
(43) Bittel, L.; Kliesch, M. Training variational quantum algorithms is np-hard. *Phys. Rev. Lett.* **2021**, *127*, 120502.
(44) Anschuetz, E. R.; Kiani, B. T. Quantum variational algorithms are swamped with traps. *Nat. Commun.* **2022**, *13*, 7760.
(45) McClean, J. R.; Boixo, S.; Smelyanskiy, V. N.; Babbush, R.; Neven, H. Barren plateaus in quantum neural network training landscapes. *Nat. Commun.* **2018**, *9*, 4812.
(46) D'Cunha, R.; Crawford, T. D.; Motta, M.; Rice, J. E. Challenges in the Use of Quantum Computing Hardware-Efficient Ansätze in Electronic Structure Theory. *J. Phys. Chem. A* **2023**, *127*, 3437−3448.
(47) Motta, M.; Sung, K. J.; Whaley, K. B.; Head-Gordon, M.; Shee, J. Bridging physical intuition and hardware efficiency for correlated electronic states: the local unitary cluster Jastrow ansatz for electronic structure. *ChemRxiv* **2023**. preprint
(48) Kaplan, A. D.; Levy, M.; Perdew, J. P. The predictive power of exact constraints and appropriate norms in density functional theory. *Annu. Rev. Phys. Chem.* **2023**, *74*, 193−218.
(49) Perdew, J. P.; Burke, K.; Ernzerhof, M. Generalized gradient approximation made simple. *Phys. Rev. Lett.* **1996**, *77*, 3865−3868.
(50) Sun, J.; Ruzsinszky, A.; Perdew, J. P. Strongly constrained and appropriately normed semilocal density functional. *Phys. Rev. Lett.* **2015**, *115*, 036402.
(51) Cybenko, G. Approximation by superpositions of a sigmoidal function. *Math. Control, Signals, Syst.* **1989**, *2*, 303−314.
(52) Hornik, K.; Stinchcombe, M.; White, H. Multilayer feedforward networks are universal approximators. *Neural Networks* **1989**, *2*, 359−366.
(53) He, K.; Zhang, X.; Ren, S.; Sun, J. Deep residual learning for image recognition *Proceedings of the IEEE Conference on Computer Vision and Pattern Recognition*, 2016; pp 770−778.
(54) Pople, J. A.; Binkley, J. S.; Seeger, R. Theoretical models incorporating electron correlation. *Int. J. Quantum Chem.* **1976**, *10*, 1−19.
(55) Bartlett, R. J. Many-body perturbation theory and coupled cluster theory for electron correlation in molecules. *Annu. Rev. Phys. Chem.* **1981**, *32*, 359−401.
(56) Nooijen, M.; Shamasundar, K.; Mukherjee, D. Reflections on size-extensivity, size-consistency and generalized extensivity in many-body theory. *Mol. Phys.* **2005**, *103*, 2277−2298.
(57) Barkoutsos, P. K.; Gonthier, J. F.; Sokolov, I.; Moll, N.; Salis, G.; Fuhrer, A.; Ganzhorn, M.; Egger, D. J.; Troyer, M.; Mezzacapo, A.; et al. Quantum algorithms for electronic structure calculations: Particle-hole hamiltonian and optimized wave-function expansions. *Phys. Rev. A* **2018**, *98*, 022322.
(58) Gard, B. T.; Zhu, L.; Barron, G. S.; Mayhall, N. J.; Economou, S. E.; Barnes, E. Efficient symmetry-preserving state preparation circuits for the variational quantum eigensolver algorithm. *npj Quantum Inf.* **2020**, *6*, 10.
(59) Kottmann, J. S.; Aspuru-Guzik, A. Optimized low-depth quantum circuits for molecular electronic structure using a separable-pair approximation. *Phys. Rev. A* **2022**, *105*, 032449.
(60) Kottmann, J. S. Molecular quantum circuit design: A graph-based approach. *Quantum* **2023**, *7*, 1073.
(61) Eddins, A.; Motta, M.; Gujarati, T. P.; Bravyi, S.; Mezzacapo, A.; Hadfield, C.; Sheldon, S. Doubling the size of quantum simulators by entanglement forging. *PRX Quantum* **2022**, *3*, 010309.
(62) Cai, X.; Fang, W.-H.; Fan, H.; Li, Z. Quantum computation of molecular response properties. *Phys. Rev. Res.* **2020**, *2*, 033324.
(63) Huang, K.; Cai, X.; Li, H.; Ge, Z. Y.; Hou, R.; Li, H.; Liu, T.; Shi, Y.; Chen, C.; Zheng, D.; et al. Variational Quantum Computation of Molecular Linear Response Properties on a Superconducting Quantum Processor. *J. Phys. Chem. Lett.* **2022**, *13*, 9114−9121.
(64) Nielsen, M. A.; Chuang, I. L. *Quantum Computation and Quantum Information*; Cambridge University Press, 2010.
(65) Evangelista, F. A.; Chan, G. K.-L.; Scuseria, G. E. Exact parameterization of fermionic wave functions via unitary coupled cluster theory. *J. Chem. Phys.* **2019**, *151*, 244112.
(66) Kjaergaard, M.; Schwartz, M. E.; Braumüller, J.; Krantz, P.; Wang, J. I.-J.; Gustavsson, S.; Oliver, W. D. Superconducting qubits: Current state of play. *Annu. Rev. Condens. Matter Phys.* **2020**, *11*, 369−395.
(67) Vidal, G.; Dawson, C. M. Universal quantum circuit for two-qubit transformations with three controlled-NOT gates. *Phys. Rev. A: At., Mol., Opt. Phys.* **2004**, *69*, 010301.
(68) Vatan, F.; Williams, C. Optimal quantum circuits for general two-qubit gates. *Phys. Rev. A: At., Mol., Opt. Phys.* **2004**, *69*, 032315.
(69) Foxen, B.; Neill, C.; Dunsworth, A.; Roushan, P.; Chiaro, B.; Megrant, A.; Kelly, J.; Chen, Z.; Satzinger, K.; Barends, R.; et al. Demonstrating a continuous set of two-qubit gates for near-term quantum algorithms. *Phys. Rev. Lett.* **2020**, *125*, 120504.
(70) MindQuantum Developer. *MindQuantum*, Version 0.6.0, 2021. https://gitee.com/mindspore/mindquantum.
(71) Virtanen, P.; Gommers, R.; Oliphant, T. E.; Haberland, M.; Reddy, T.; Cournapeau, D.; Burovski, E.; Peterson, P.; Weckesser, W.; Bright, J.; et al. SciPy 1.0: fundamental algorithms for scientific computing in Python. *Nat. Methods* **2020**, *17*, 261−272.
(72) Sun, Q.; Berkelbach, T. C.; Blunt, N. S.; Booth, G. H.; Guo, S.; Li, Z.; Liu, J.; McClain, J. D.; Sayfutyarova, E. R.; Sharma, S.; Wouters, S.; Chan, G. K.-L. PySCF: the Python-based simulations of chemistry framework. *Wiley Interdiscip. Rev. Comput. Mol. Sci.* **2018**, *8*, No. e1340.
(73) Jordan, P.; Wigner, E. About the Pauli exclusion principle. *Z. Phys.* **1928**, *47*, 631−651.
(74) McClean, J. R.; Rubin, N. C.; Sung, K. J.; Kivlichan, I. D.; Bonet-Monroig, X.; Cao, Y.; Dai, C.; Fried, E. S.; Gidney, C.; Gimby, B.; et al. OpenFermion: the electronic structure package for quantum computers. *Quantum Sci. Technol.* **2020**, *5*, 034014.
(75) Arute, F.; Arya, K.; Babbush, R.; Bacon, D.; Bardin, J. C.; Barends, R.; Boixo, S.; Broughton, M.; Buckley, B. B.; Buell, D. A.; Burkett, B.; Bushnell, N.; Chen, Y.; Chen, Z.; Chiaro, B.; Collins, R.; Courtney, W.; Demura, S.; Dunsworth, A.; Farhi, E.; Fowler, A.; Foxen, B.; Gidney, C.; Giustina, M.; Graff, R.; Habegger, S.; Harrigan, M. P.; Ho, A.; Hong, S.; Huang, T.; Huggins, W. J.; Ioffe, L.; Isakov, S. V.; Jeffrey, E.; Jiang, Z.; Jones, C.; Kafri, D.; Kechedzhi, K.; Kelly, J.; Kim, S.; Klimov, P. V.; Korotkov, A.; Kostritsa, F.; Landhuis, D.; Laptev, P.; Lindmark, M.; Lucero, E.; Martin, O.; Martinis, J. M.; McClean, J. R.; McEwen, M.; Megrant, A.; Mi, X.; Mohseni, M.; Mruczkiewicz, W.; Mutus, J.; Naaman, O.; Neeley, M.; Neill, C.; Neven, H.; Niu, M. Y.; O'Brien, T. E.; Ostby, E.; Petukhov, A.; Putterman, H.; Quintana, C.; Roushan, P.; Rubin, N. C.; Sank, D.; Satzinger, K. J.; Smelyanskiy, V.; Strain, D.; Sung, K. J.; Szalay, M.; Takeshita, T. Y.; Vainsencher, A.; White, T.; Wiebe, N.; Yao, Z. J.; Yeh, P.; Zalcman, A. Hartree-Fock on a superconducting qubit quantum computer. *Science* **2020**, *369*, 1084−1089.
(76) Magoulas, I.; Evangelista, F. A. Linear-Scaling Quantum Circuits for Computational Chemistry. *arXiv* **2023**, arXiv:2304.12870. preprint

https://doi.org/10.1021/acs.jctc.3c00966
J. Chem. Theory Comput. 2024, 20, 1912−1922